Society for Mathematical Biology

ORIGINAL PAPER



Modeling Intracellular Delay in Within-Host HIV Dynamics Under Conditioning of Drugs of Abuse

Naveen K. Vaidya¹ • Michael Peter²

Received: 21 September 2020 / Accepted: 5 May 2021 © The Author(s), under exclusive licence to Society for Mathematical Biology 2021

Abstract

Drugs of abuse, such as opiates, have been widely associated with the enhancement of HIV replication, the acceleration of disease progression, and severe neuropathogenesis. Specifically, the presence of drugs of abuse (morphine) switches target cells (CD4+ T cells) from lower-to-higher susceptibility to HIV infection. The effect of such switching behaviors on viral dynamics may be altered due to the intracellular delay (the replication time between viral entry into a target cell and the production of new viruses by the infected cell). In this study, we develop, for the first time, a viral dynamics model that includes an intracellular delay under the conditioning of drugs of abuse. We parameterize the model using experimental data from simian immunodeficiency virus infection of morphine-addicted macaques. Results from thorough mathematical analyses and numerical simulations of our model show that the intracellular delay can play a significant role in HIV dynamics under the conditioning of drugs of abuse, particularly during the acute phase of infection. Our model and the related results provide new insights into the HIV dynamics and may help develop strategies to control HIV infections in drug abusers.

Keywords Delay differential equations · Drugs of abuse · HIV Infection · Intracellular delay · Stability analysis

Naveen K. Vaidya nvaidya@sdsu.edu

> Michael Peter michael_peter1@web.de

Published online: 01 June 2021

Department of Mathematics and Statistics, San Diego State University, 5500 Campanile Dr, San Diego, CA 92182, USA



Department of Mathematics and Statistics, Computational Science Research Center, Viral Information Institute, San Diego State University, 5500 Campanile Dr, San Diego, CA 92182, USA

81 Page 2 of 23 N. K. Vaidya, M. Peter

1 Introduction

Human immunodeficiency virus (HIV) remains an ongoing public health challenge across the globe. Worldwide, over 37 million people are currently living with the virus. Approximately 1.8 million new infections and one million HIV-related deaths occur annually (Avert 2018; Joint United Nations Programme on HIV and AIDS 2018). HIV is a retrovirus that invades the human body and attacks the immune system responsible for fighting against various infections in the body. Individuals infected with HIV can eventually progress to acquired immunodeficiency syndrome (AIDS). At AIDS, the immune system is severely weakened to fight off opportunistic infections, which may lead to the patient's death (U.S. Department of Health and Human Services 2018b).

HIV spreads through contact with certain body fluids from a person infected with HIV. The most common modes of viral transmission are sexual intercourse, contaminated blood transfusion, and needle sharing among drug abusers (Levy 1993; U.S. Department of Health and Human Services 2018a). Drug abusers constitute one of the major portions of HIV infected population within the USA and other parts of the world. In 2017, people who inject drugs accounted for approximately 10% of HIV diagnoses in the USA (Centers for Disease Control and Prevention 2019), and a third of 1.1 million US residents who are currently living with HIV use drugs or binge on alcohol (National Institute on Drug Abuse 2015; U.S. Department of Health and Human Services 2019). These statistics show that drugs of abuse are a significant problem among HIV infected individuals. Conditioning of drugs of abuse has been shown to exacerbate HIV infections, including a higher viral load, rapid disease progression, and higher HIV-associated neurocognitive disorders (HAND) (Kumar et al. 2004; Wang et al. 2012; Friedman et al. 2003). One of the effects that conditioning of drugs of abuse has on CD4⁺ target cells is an upregulated expression of co-receptors in these cells. HIV interacts with chemokine co-receptors of the target cell, such as CCR5 or CXCR4, to effectively bind to the target cell and eventually enter it. Increasing the expression of these co-receptors due to drugs of abuse such as morphine leads to a higher susceptibility of the CD4⁺ target cells (Guo et al. 2002; Li et al. 2003; Suzuki et al. 2002).

Mathematical models have been widely used to provide insights into the dynamics of infectious diseases, including viral dynamics (Perelson and Ribeiro 2013; Nowak and May 2000; Bonhoeffer et al. 1997; Stafford et al. 2000; Vaidya et al. 2018). Vaidya et al. (2016) modeled the effect of morphine on HIV dynamics by introducing an additional target cell subpopulation of higher susceptibility due to upregulated co-receptor expression in the presence of morphine. Their model can explain the experimental observation that the presence of morphine can cause a higher viral set point and a higher loss of CD4⁺ T cells. However, in their model, it was assumed that viral replication occurs instantaneously, ignoring the intracellular delay, the time required for this replication process to complete. This intracellular delay represents the actual time from the virus entry into a target cell to the time of virions being released from the infected cells (Nelson et al. 2000). Since target cells dynamically switch between two subpopulations during the intracellular delay, the viral dynamics may be affected by the intracellular delay in the presence of morphine.



In this study, we develop a novel viral dynamics model that includes, for the first time, the effects of intracellular delay on HIV dynamics under the conditioning of morphine. In the absence of morphine, it has already been shown that the intracellular delay can alter the stability of equilibria and initiate otherwise stable populations to fluctuate (Cai et al. 2009). We are interested in examining whether there is a similar behavior in the presence of morphine as well. We analyze our delay differential equation model, derive the basic reproduction number, and perform numerical simulations to evaluate how intracellular delay affects viral load, CD4 count, and subpopulation switch in the presence of morphine.

2 Model

We extend a previous SIV dynamics model under morphine conditioning (Vaidya et al. 2016) by including an intracellular delay. We focus on upregulated co-receptor expression in the target cells (CD4⁺ T cells) due to morphine concentration. We do not include the effect of morphine on the immune response since our main goal is to examine the acute phase of HIV infection, where immune responses are primarily absent (Mutua et al. 2019). As in the previous models (Li and Shu 2010; Nelson et al. 2000; Zhu and Zou 2009; Herz et al. 1996), we introduce the intracellular phase of the virus life-cycle through a constant delay τ , which represents the time lag between the time the virus enters a target cell and the time the infected cell produces virions. Because of this intracellular delay, the virus-producing cells (I) at time t are those target cells into which the virus successfully enters at time $t-\tau$ and are still alive at time t. Assuming a constant death rate s during the delay phase for an initially infected cell but not yet producing virus, the survival probability of these cells from time $t-\tau$ to t is given by $e^{-s\tau}$. As in Vaidya et al. (2016), we consider two subpopulations of target cells with different susceptibility and allow the cells to switch between these two subpopulations. As a result, the ratio between higher susceptible target cells (T_h) and lower susceptible target cells (T_1) at time $t - \tau$ might differ from the ratio at time t. The model is described by the following set of delay-differential equations:

$$\frac{dT_{l}(t)}{dt} = \lambda + qT_{h}(t) - dT_{l}(t) - rT_{l}(t) - \beta_{l}V(t)T_{l}(t),
\frac{dT_{h}(t)}{dt} = rT_{l}(t) - dT_{h}(t) - qT_{h}(t) - \beta_{h}V(t)T_{h}(t),
\frac{dI(t)}{dt} = \beta_{l}V(t - \tau)T_{l}(t - \tau)e^{-s\tau} + \beta_{h}V(t - \tau)T_{h}(t - \tau)e^{-s\tau} - \delta I(t),
\frac{dV(t)}{dt} = pI(t) - cV(t),$$
(1)

with initial conditions and history

$$T_1(t) = T_{l0}, \quad t \in [-\tau, 0],$$

 $T_h(t) = T_{h0}, \quad t \in [-\tau, 0],$



81 Page 4 of 23 N. K. Vaidya, M. Peter

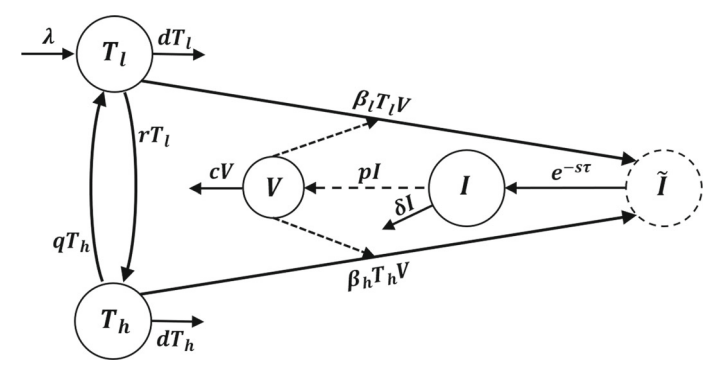


Fig. 1 Schematic diagram of the delay model of HIV infection under morphine conditioning. The model contains two subpopulations of target cells: one with higher susceptibility, $T_{\rm h}$ and another with lower susceptibility, $T_{\rm l}$. Cells can switch between these populations with transition rates r from $T_{\rm l}$ to $T_{\rm h}$ and q from $T_{\rm h}$ to $T_{\rm l}$. Both target cell populations die at per capita rate d and become initially infected cells, \tilde{I} , upon contact with the free virus, V, at rates $\beta_{\rm l}$ and $\beta_{\rm h}$, respectively. Initially, infected cells survive the intracellular delay τ with probability $e^{-s\tau}$, before they become productively infected cells, I, and produce new virions at a rate p virions per cell per day. Productively infected cells die at a rate δ per day, and virus gets cleared at rate c

$$V(t) = \begin{cases} 0, & \text{for } t \in [-\tau, 0), \\ V_0, & \text{for } t = 0, \end{cases}$$
$$I(t) = 0, \quad t \in [-\tau, 0].$$

Here, for simplicity, we assume that target cells newly recruited at a constant rate λ are all in the lower susceptible subpopulation T_1 . The per capita loss rate d is a result of the difference between loss from cell death and gain due to cell division. The transition rates from T_1 to T_h and T_h to T_1 are denoted by r and q, respectively. Lower and higher susceptible target cells can become initially infected, \tilde{I} , upon contact with the free virus, V, at rates β_1 and β_h , respectively. These initially infected cells become productively infected cells, I, with survival probability $e^{-s\tau}$ and start producing new virions at rate p virions per cell per day. Productively infected cells die at rate δ per day. The virus clearance rate is denoted by c. A schematic diagram of the model is shown in Fig. 1.

As our model is in the form of delay-differential equations, we also have to consider the history of virus and cell populations τ time units before the initial infection to obtain the solution of the model. For simplicity, we choose the history functions to be constant such that $T_1(t) = T_{l0}$ and $T_h(t) = T_{h0}$ for $t \in [-\tau, 0]$. As there are no infected cells and no virus before the primary infection at t = 0, we set these two history functions equal to 0 for t < 0. At t = 0, the infection takes place, and we assume that the infection begins with the free virus. Hence, we take $V(0) = V_0$ and I(0) = 0.

3 Data Fitting and Model Parameters

In this section, we estimate the model parameters by fitting the model solution to experimental data.



3.1 Data

The viral load data we used for the parameter estimation of our model was obtained from a published study on 12 male rhesus macaques (Kumar et al. 2004; Vaidya et al. 2016). Six of the monkeys were morphine-dependent, and the other six animals were the control group. The morphine dependence was established and maintained by injecting doses of morphine intramuscularly over 20 weeks. For the control group, a saline injection was used. All animals were infected intravenously with SIV and monitored for 12 weeks. During this time, the plasma viral load was measured at weeks 0, 1, 2, 3, 4, 6, 8, 10, and 12 after the infection.

Due to the complexity of the delay differential equation system as well as the high number of parameters to be estimated, the limited data were insufficient to properly run the data fitting. Therefore, we generated additional data points using the model in Vaidya et al. (2016), which successfully describes the experimental data from the SIV infected macaques. We considered the geometrical mean viral load data among animals from the control group and calculated the standard deviation (sd) of the residuals in the results obtained from the previous model. We then extracted 45 data points from the model solution and added noise from random, normally distributed errors with mean 0 and variance sd^2 . Using this generated data, we estimated the parameters of our delay differential equation model. We repeated the process by generating 1000 different data sets.

3.2 Parameter Estimation

Each macaque was infected intravenously with a 2-ml-inoculum containing 10⁴ TCID₅₀ of each of three chosen SIV viruses (SHIV_{KU-1B}, SHIV_{89-6P}, and SIV_{17E-Fr}) (Kumar et al. 2004). The total of 3×10^4 TCID₅₀ of viruses contains at least 3×10^5 HIV RNA copies (Ma et al. 2009). A macaque, on average, weighs 1/10 of a human, which approximately gives 1.5 liters of extracellular water in a macaque. Assuming that the infused RNA copies are dispersed into extracellular water, the initial viral load, V_0 , can be estimated as $V_0 \approx \frac{3 \times 10^5}{1.5L} \approx 200$ viral RNA copies/ml. As discussed in Vaidya et al. (2016), we take $T_{h0} = 40$, 980 and $T_{l0} = T_0 - T_{h0}$ as the initial populations of target cells, where $T_0 = 10^6$ cells/ml is the total number of CD4⁺ T cells per ml in a macaque (Kumar et al. 2004; U.S. Department of Health and Human Services 2017). Chen et al. (2007) estimated the SIV burst size in vivo in rhesus macaques as approximately 5×10^4 virions per day per infected cell. With one day average lifespan of productively infected cells (Markowitz et al. 2003) and only 5% of the total CD4 count as susceptible target cells for SIV infection in macaques (Vaidya et al. 2010), this burst size provides the virus production rate p = 2500 vRNAcell⁻¹ day⁻¹. Further, Ramratnam et al. (1999) estimated the virion clearance rate during chronic infection in humans between 9.1 and 36.0 day⁻¹, with an average of 23 day^{-1} . We, therefore, take $c = 23 day^{-1}$ as a minimal estimate and acknowledge that this value might be larger in macaques (Zhang et al. 2002). As estimated in Stafford et al. (2000), we take 100 days as the average life span of uninfected target cells, i.e., $d = 0.01 \text{ day}^{-1}$. Since there is no conclusive estimate for the death rate of ini-



81 Page 6 of 23 N. K. Vaidya, M. Peter

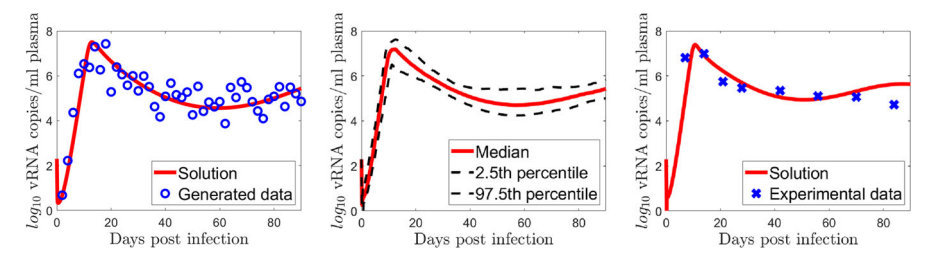


Fig. 2 Fitting of the model to generated data and experimental observations. [Left] The model prediction and one particular set of data, generated based on the model in Vaidya et al. (2016) with noise added. [Middle] The 2.5th percentile, the median, and the 97.5th percentile of the best-fit solutions corresponding to the 1000 data sets. [Right] The viral load predicted by the model (solid line) with the estimated parameters compared to the experimental data (cross)

tially infected target cells during the intracellular phase, we set s = d. The remaining parameters $(\beta_1, \beta_h, r, q, \tau, \delta, \lambda)$ are estimated by fitting the model to the data.

We solved model (1) using the delay differential equation solver "dde23" (The MathWorks Inc. 2019a) in MATLAB. The parameters were estimated by minimizing the residual sum of squares between the model solution and the generated viral load data with the MATLAB optimization function "fmincon" (The MathWorks Inc. 2019b). By generating 1,000 sets of data and fitting the model to each of them, we computed 95% confidence intervals for the estimated parameters. The estimated parameters, their parameter descriptions, and confidence intervals are summarized in Table 1. In Fig. 2, we present the fitting of the model to generated data, showing that the curve fits the generated data well. The small confidence interval of the estimated parameter assures reasonable parameter estimates. Furthermore, we compared the model solution for the estimated parameters with the experimental data and observed a good agreement between them (Fig. 2).

4 Model Analysis

To investigate the dynamics of system (1), we first consider suitable phase space and a feasible region. For $\tau > 0$, we consider $\mathbb{X} = C([-\tau, 0], \mathbb{R})$, the Banach space of continuous functions from $[-\tau, 0]$ into \mathbb{R} , with norm $||\Phi|| = \sup_{-\tau \le t \le 0} |\Phi(t)|$ for $\Phi \in \mathbb{X}$. The nonnegative cone of \mathbb{X} is defined as $\mathbb{X}^+ = C([-\tau, 0], \mathbb{R}_+)$.

4.1 Positivity and Boundedness of Solutions

We first establish the positivity and boundedness of solutions of (1) in the following theorem.

Theorem 1 With the initial conditions $\Psi(0)$ chosen from $\mathbb{X}^+ \times \mathbb{X}^+ \times \mathbb{R}_+ \times \mathbb{X}^+$ with $\Psi(0) > 0$, all solutions of system (1) are positive and ultimately bounded.

Proof We implement the method of contradiction to prove the positivity of the solutions. If possible, suppose that $T_1(t) > 0$ for all t > 0 is not true, and let $t_{l1} > 0$



Table 1 Initial values and parameters. The values along with their 95% confidence intervals obtained from the data fitting

Sym.	Description	Value [Confidence Interval]	Sources
Initial valu	ies		
T_{l0}	Low susceptible CD4 ⁺ target cells	959,020 ml ⁻¹	Vaidya et al. (2016)
T_{h0}	High susceptible CD4 ⁺ target cells	$40,980 \text{ml}^{-1}$	Vaidya et al. (2016)
I_0	Infected CD4 ⁺ target cells	0 ml^{-1}	Assumption, Stafford et al. (2000), Vaidya et al. (2016)
V_0	Viral RNA copies	200 ml^{-1}	Derived, Kumar et al. (2004), Ma et al. (2009)
Parameter			
p	Virus production rate	2500 vRNA cell ⁻¹ day ⁻¹	Derived, Chen et al. (2007), Markowitz et al. (2003), Vaidya et al. (2010)
c	Virus clearance rate	23 day^{-1}	Ramratnam et al. (1999)
d	Uninfected target cell death rate	$0.01 \mathrm{day}^{-1}$	Stafford et al. (2000)
S	Initially infected target cell death rate ³	$0.01 \; {\rm day}^{-1}$	Assumption
δ	Productively infected target cell death rate	$0.795 \mathrm{day}^{-1}$	Data fitting
		[0.408, 1.984]	
λ	Constant production rate of T_1 cells	$3689.99 \text{ ml}^{-1} \text{day}^{-1}$	Data fitting
		[3659.58, 3690.26]	
r	Transition rate from T_1 to T_h	$0.205 \; \mathrm{day^{-1}}$	Data fitting
		[0.104, 0.319]	
q	Transition rate from T_h to T_l	$0.239 \mathrm{day}^{-1}$	Data fitting
		[0.085, 0.996]	
$eta_{ m l}$	Infection rate of T_1 cells	1.03×10^{-11} vRNA/day	Data fitting
		$[1.00 \times 10^{-11}, 1.46 \times 10^{-11}]$	
$eta_{ m h}$	Infection rate of T_h cells	1.04×10^{-7} vRNA/day	Data fitting
		$[4.48 \times 10^{-8}, 5.63 \times 10^{-7}]$	
τ	Intracellular delay	0.231 days [0.031, 0.704]	Data fitting

During intracellular phase of viral replication



81 Page 8 of 23 N. K. Vaidya, M. Peter

be the first time point such that $T_l(t_{l1}) = 0$. Then, form the first equation of system (1), we obtain $\frac{dT_l}{dt}\Big|_{t=t_{l1}} = \lambda + qT_h(t_{l1})$. We claim that $T_h(t_{l1})$ cannot be negative. If $T_h(t_{l1}) < 0$, we can find the first time point $t_{h1} \in [0, t_{l1})$ such that $T_h(t_{h1}) = 0$. Then, the second equation of system (1) provides $\frac{dT_h}{dt}\Big|_{t=t_{h1}} = rT_l(t_{h1})$. Since $t_{h1} < t_{l1}$, $T_l(t_{h1}) > 0$, which provides $\frac{dT_h}{dt}\Big|_{t=t_{h1}} > 0$. This implies that $T_h(t) < 0$ for t in $(t_{h1} - \epsilon_{h1}, t_{h1})$, where ϵ_{h1} is sufficiently small. This contradicts $T_h(t) > 0$ for $t \in [0, t_{h1})$. This follows that $T_h(t_{l1}) \geq 0$, which provides $\frac{dT_l}{dt}\Big|_{t=t_{l1}} > 0$. This implies that $T_l(t) < 0$ for t in $(t_{l1} - \epsilon_{l1}, t_{l1})$, where ϵ_{l1} is sufficiently small. This contradicts $T_l(t) > 0$ for $t \in [0, t_{l1})$. Therefore, $T_l(t) > 0$ for t > 0. This also implies that $T_h(t) > 0$ for t > 0. Otherwise, the first time point t_{h2} with $T_h(t_{h2}) = 0$ along with the second equation of system (1) provides $\frac{dT_h}{dt}\Big|_{t=t_{h2}} = rT_l(t_{h2}) > 0$. This again implies that $T_h(t) < 0$ for t in $(t_{h2} - \epsilon_{h2}, t_{h2})$, where ϵ_{h2} is sufficiently small, contradicting $T_h(t) > 0$ for $t \in [0, t_{h2})$. Hence we conclude that $T_l(t) > 0$, $T_h(t) > 0$ for t > 0. Similarly, we apply the method of contradiction to show the solutions I(t) and V(t)

Similarly, we apply the method of contradiction to show the solutions I(t) and V(t) of system (1) are positive for t > 0. If V(t) > 0 for all t > 0 is not true, we can find the first time point $t_{v1} > 0$ such that $V(t_{v1}) = 0$. Then, the fourth equation of system (1) provides $\frac{\mathrm{d}v}{\mathrm{d}t}\Big|_{t=t_{v1}} = pI(t_{v1})$. Also, from the third equation of system (1), we get

$$I(t_{v1}) = e^{-\delta t_{v1}} \left[I(0) + \int_0^{t_{v1}} \{ \beta_1 T_1(\eta - \tau) + \beta_h T_h(\eta - \tau) \} V(\eta - \tau) e^{-s\tau + \delta \eta} d\eta \right]$$

$$> 0.$$

This implies that $\frac{dV}{dt}\Big|_{t=t_{v1}} > 0$, and with the same argument as above we get V(t) > 0 for t > 0. Furthermore, we obtain

$$I(t) = e^{-\delta t} \left[I(0) + \int_0^t \left\{ \beta_1 T_1(\eta - \tau) + \beta_h T_h(\eta - \tau) \right\} V(\eta - \tau) e^{-s\tau + \delta \eta} d\eta \right]$$
> 0.

This completes the proof of the positivity of the solutions of system (1).

To prove the boundedness, we first assume $T = T_1 + T_h$, and then from the first two equations of (1), we get

$$\frac{\mathrm{d}T(t)}{\mathrm{d}t} = \lambda - dT(t) - [\beta_1 T_1(t) + \beta_h T_h(t)]V(t) \le \lambda - dT(t).$$

This implies $\limsup_{t\to\infty} T(t) \leq \frac{\lambda}{d}$, and consequently $\limsup_{t\to\infty} T_{\mathrm{l}}(t) \leq \frac{\lambda}{d}$ and $\limsup_{t\to\infty} T_{\mathrm{h}}(t) \leq \frac{\lambda}{d}$. Then, from the first three equations of (1), we obtain

$$\frac{\mathrm{d}}{\mathrm{d}t} \left[T_{\mathrm{l}}(t) + T_{\mathrm{h}}(t) + I(t+\tau) \right] = \lambda - d[T_{\mathrm{l}}(t) + T_{\mathrm{h}}(t)] - \delta I(t+\tau)$$



+
$$[\beta_1 T_1(t) + \beta_h T_h(t)]V(t)(e^{-s\tau} - 1)$$

< $\lambda - d_{\min}[T_1(t) + T_h(t) + I(t + \tau)],$

where $d_{\min} = \min\{d, \delta\}$. Here, we can take $d_{\min} = d$ as the life-span of infected cell (~ 1 day) is extremely shorter than the life-span of uninfected cell (~ 100 days), i.e., $d << \delta$. Thus, $\limsup_{t\to\infty} [T_1(t) + T_h(t) + I(t+\tau)] \le \frac{\lambda}{d}$. Then, from the last equation of (1), we obtain

$$\frac{\mathrm{d}V(t)}{\mathrm{d}t} = pI(t) - cV(t) \le p\frac{\lambda}{d} - cV(t)$$

which implies $\limsup_{t\to\infty}V(t)\leq \frac{p\lambda}{dc}$. Therefore, $T_{l}(t)$, $T_{h}(t)$, I(t), and V(t) are ultimately bounded in $\mathbb{X}^{+}\times\mathbb{X}^{+}\times\mathbb{R}_{+}\times\mathbb{X}^{+}$.

Using above conditions, we observe that the dynamics of system (1) can be analyzed in the following bounded feasible region

$$\Omega = \left\{ (T_1, T_h, I, V) \in \mathbb{X}^+ \times \mathbb{X}^+ \times \mathbb{R}_+ \times \mathbb{X}^+ : ||T_1 + T_h|| \le \frac{\lambda}{d}, \\ ||T_1 + T_h + I|| \le \frac{\lambda}{d}, ||V|| \le \frac{p\lambda}{dc} \right\}.$$

Moreover, the region Ω is positively invariant with respect to model (1).

We now compute and analyze the basic reproduction number R_0 . We also study the equilibria of the model and their stability.

4.2 Infection Free Equilibrium and Basic Reproduction Number

The basic reproduction number, R_0 , is the average number of secondary infected cells resulted from one infected cell in its lifetime. We derive R_0 by computing the dominate eigenvalue of the next-generation operator (Diekmann et al. 1990; Van den Driessche and Watmough 2002; Heffernan et al. 2005; Nakata and Omori 2015) while we acknowledge that there may be other methods. In the absence of HIV infection, i.e., I = V = 0, model (1) reduces to

$$\begin{aligned} \frac{\mathrm{d}T_{\mathrm{l}}(t)}{\mathrm{d}t} &= \lambda + qT_{\mathrm{h}}(t) - dT_{\mathrm{l}}(t) - rT_{\mathrm{l}}(t), \\ \frac{\mathrm{d}T_{\mathrm{h}}(t)}{\mathrm{d}t} &= rT_{\mathrm{l}}(t) - dT_{\mathrm{h}}(t) - qT_{\mathrm{h}}(t). \end{aligned}$$

By setting the equations above equal to 0, we obtain the unique infection free equilibrium $E^0 = (T_1^0, T_h^0, 0, 0)$, where

$$T_{\mathrm{l}}^{0} = \frac{\lambda(d+q)}{d(d+q+r)}, \quad T_{\mathrm{h}}^{0} = \frac{\lambda r}{d(d+q+r)}.$$



81 Page 10 of 23 N. K. Vaidya, M. Peter

In model (1) we have two infected compartments I and V. We define $y_1 = I$, $y_2 = V$,

$$\begin{split} \mathcal{F}_{1}(t) &= \beta_{1}V(t-\tau)T_{1}(t-\tau)e^{-s\tau} \\ &+ \beta_{h}V(t-\tau)T_{h}(t-\tau)e^{-s\tau}, \qquad \qquad \mathcal{V}_{1}(t) = \delta I(t), \\ \mathcal{F}_{2}(t) &= 0, \qquad \qquad \mathcal{V}_{2}(t) = -pI(t) + cV(t). \end{split}$$

We now introduce two matrices

$$\mathbb{F} = \begin{bmatrix} \frac{\partial \mathcal{F}_i}{\partial y_j} \left(E^0 \right) \end{bmatrix} \qquad = \begin{pmatrix} 0 & \frac{\lambda}{d(d+q+r)} [\beta_1(d+q) + \beta_h r] e^{-s\tau} \\ 0 & 0 \end{pmatrix} \\
\mathbb{V} = \begin{bmatrix} \frac{\partial \mathcal{V}_i}{\partial y_j} \left(E^0 \right) \end{bmatrix} \qquad = \begin{pmatrix} \delta & 0 \\ -p & c \end{pmatrix} \implies \mathbb{V}^{-1} = \frac{1}{\delta c} \begin{pmatrix} c & 0 \\ p & \delta \end{pmatrix}$$

These expressions give

$$\mathbb{FV}^{-1} = \begin{pmatrix} \frac{\lambda p}{\delta c d(d+q+r)} [\beta_{l}(d+q) + \beta_{h}r] e^{-s\tau} & \frac{\lambda}{c d(d+q+r)} [\beta_{l}(d+q) + \beta_{h}r] e^{-s\tau} \\ 0 & 0 \end{pmatrix}$$

and R_0 corresponds to the spectral radius of \mathbb{FV}^{-1} :

$$R_0 = \rho\left(\mathbb{FV}^{-1}\right) = \frac{\lambda p}{\delta c d(d+q+r)} [\beta_{\mathrm{l}}(d+q) + \beta_{\mathrm{h}} r] e^{-s\tau}.$$

Rewriting this formula leads to a more heuristic approach previously implemented (Li and Shu 2010) to derive the basic reproduction number for delay differential equation model of within-host viral dynamics:

$$\begin{split} R_0 &= \frac{\lambda(d+q)}{d(d+q+r)} \cdot \frac{p}{\delta} \cdot \frac{\beta_1 e^{-s\tau}}{c} + \frac{\lambda r}{d(d+q+r)} \cdot \frac{p}{\delta} \cdot \frac{\beta_1 e^{-s\tau}}{c} \\ &= T_1^0 \cdot \frac{p}{\delta} \cdot \frac{\beta_1 e^{-s\tau}}{c} + T_1^0 \cdot \frac{p}{\delta} \cdot \frac{\beta_1 e^{-s\tau}}{c} \end{split}$$

Note, an infected target cell produces $\frac{p}{\delta}$ virions over its entire lifetime $\frac{1}{\delta}$. Each of these virions can infect T_1^0 and T_h^0 susceptible target cells at a rate of $\frac{\beta_1}{c}$ or $\frac{\beta_h}{c}$, respectively, over its life span $\frac{1}{c}$. Out of these initially infected cells only a fraction $e^{-s\tau}$ survives the delay period τ to become infectious and start producing virus. Therefore, the total number of secondary productively infected cells from one initial infected cell is $T_1^0 \cdot \frac{p}{\delta} \cdot \frac{\beta_1 e^{-s\tau}}{c} + T_h^0 \cdot \frac{p}{\delta} \cdot \frac{\beta_1 e^{-s\tau}}{c}$, which is equal to R_0 derived above.

4.3 Stability Analysis of the Infection Free Equilibrium

We will prove the local stability of E^0 in the following theorem.



Theorem 2 The infection-free equilibrium E^0 is locally asymptotically stable if $R_0 < 1$ and unstable if $R_0 > 1$.

Proof For convenience, we let $\overrightarrow{u}(t)$ be the transpose of vector $(T_1(t), T_h(t), I(t), V(t))$. Linearizing the model system (1) at E^0 , we obtain

$$\frac{d}{dt}\overrightarrow{u}(t) = \mathbb{A}^{0}_{4\times4}\overrightarrow{u}(t) + \mathbb{B}^{0}_{4\times4}\overrightarrow{u}(t-\tau),\tag{2}$$

with

$$\mathbb{A}^0_{4\times 4} = \begin{pmatrix} W^0_{2\times 2} & X^0_{2\times 2} \\ 0_{2\times 2} & Y^0_{2\times 2} \end{pmatrix}, \quad \mathbb{B}^0_{4\times 4} = \begin{pmatrix} 0_{2\times 2} & 0_{2\times 2} \\ 0_{2\times 2} & Z^0_{2\times 2} \end{pmatrix},$$

where

$$\begin{split} W^{0} &= \begin{pmatrix} -d-r & q \\ r & -d-q \end{pmatrix}, \quad X^{0} &= \begin{pmatrix} 0 & -\beta_{1}T_{1}^{0} \\ 0 & -\beta_{h}T_{h}^{0} \end{pmatrix}, \quad Y^{0} &= \begin{pmatrix} -\delta & 0 \\ p & -c \end{pmatrix}, \\ Z^{0} &= \begin{pmatrix} 0 & (\beta_{1}T_{1}^{0} + \beta_{h}T_{h}^{0})e^{-s\tau} \\ 0 & 0 \end{pmatrix}. \end{split}$$

Denoting eigenvalues by ζ , the characteristic equation for (2) is

$$\Delta(\zeta) = \det[\zeta \mathbb{I}_{4\times 4} - \mathbb{A}^0 - e^{-\zeta \tau} \mathbb{B}^0] = 0$$

$$\Rightarrow \det[\zeta \mathbb{I}_{2\times 2} - W^0] \cdot \det[\zeta \mathbb{I}_{2\times 2} - Y^0 - e^{-\zeta \tau} Z^0] = 0,$$

where \mathbb{I} represents identity matrix. Since d, q, r > 0, it holds that

$$trace(W^0) = -(2d + r + q) < 0,$$

 $det(W^0) = (-d - r)(-d - q) - rq = d(d + q + r) > 0.$

Therefore, both eigenvalues of \mathbb{W}^0 are negative. Hence the stability of \mathbb{E}^0 is determined by the roots of equation

$$\det[\zeta \mathbb{I}_{2 \times 2} - Y^0 - e^{-\zeta \tau} Z^0] = 0,$$

which reduces to

$$\zeta^{2} + (c+\delta)\zeta + c\delta(1 - R_{0}e^{-\zeta\tau}) = 0.$$
 (3)

If $R_0 < 1$, then $\zeta = 0$ is not a root of (3) because $c\delta(1 - R_0) > 0$. When $\tau = 0$, (3) becomes

$$\zeta^{2} + (c + \delta)\zeta + c\delta(1 - R_{0}) = 0.$$
(4)



81 Page 12 of 23 N. K. Vaidya, M. Peter

In this case, $R_0 < 1$ implies $c\delta(1 - R_0) > 0$ under which all roots of (4) have negative real parts.

Note that all roots of (3) depend continuously on τ (Busenberg and Cooke 1993). We denote $\zeta = \chi(\tau) + i\omega(\tau)$, $(\omega > 0)$. As mentioned above $\chi(0) < 0$. Also, as in some previous studies (Beretta and Kuang 2002; Zhu and Zou 2009), we can assure that $Re(\zeta) < +\infty$ for any root of (3). Therefore, as the delay τ increases, the roots of (3) can only enter the right half in complex plane by crossing the imaginary axis. Here, $\zeta = i\omega$ with $\omega > 0$ is a purely imaginary root of (3) if and only if

$$-\omega^2 + i\omega(c+\delta) + c\delta(1 - R_0e^{-i\omega\tau}) = 0.$$

Separating the real and imaginary parts, we get

$$-\omega^2 + c\delta = c\delta R_0 \cos \omega \tau,$$

$$\omega(c+\delta) = -c\delta R_0 \sin \omega \tau.$$
 (5)

Squaring and adding these two equations, we obtain

$$\omega^4 + (c^2 + \delta^2)\omega^2 + c^2\delta^2(1 - R_0^2) = 0.$$
 (6)

If $R_0 < 1$, then $c^2 \delta^2 (1 - R_0^2) > 0$, and also $c^2 + \delta^2 > 0$. This implies that (6) has no nonnegative real root. Therefore, there is no root $\zeta = i\omega$ with $\omega > 0$ for (3), implying that the roots of (3) cannot cross the purely imaginary axis. Hence, all roots of (3) have negative real parts provided $R_0 < 1$.

On the other hand, if $R_0 > 1$, then $c^2 \delta^2 (1 - R_0^2) < 0$. In this case, (6) has a positive root ω_0 such that

$$\omega_0^2 = \frac{1}{2} \left\{ -(c^2 + \delta^2) + \sqrt{(c^2 + \delta^2)^2 + 4c^2 \delta^2 (R_0^2 - 1)} \right\}.$$

From (5), we have

$$\tau_j = \frac{1}{\omega_0} \arctan\left(\frac{\omega_0[c+\delta]}{\omega_0^2 - c\delta}\right) + \frac{2\pi}{\omega_0}j, \quad j = 0, 1, 2, \dots$$

Also, differentiation of (3) and algebraic simplification allow us to show

$$\left. \frac{\mathrm{d}}{\mathrm{d}\tau} \chi(\tau) \right|_{\tau = \tau_0} = \left. \frac{\mathrm{d}}{\mathrm{d}\tau} Re \zeta(\tau) \right|_{\tau = \tau_0} > 0.$$

By continuity, $\chi(\tau)$ becomes positive when $\tau > \tau_0$ and the infection free equilibrium, E^0 , becomes unstable. This completes the proof.



4.4 Infected Equilibrium

Using symbolic computation in MATLAB, we found two other possible equilibria $E^* = (T_1^*, T_h^*, I^*, V^*)$ and $E^{**} = (T_1^{**}, T_h^{**}, I^{**}, V^{**})$ in addition to the infection-free equilibrium, E^0 :

$$\begin{split} T_{\mathrm{l}}^* &= \frac{A - \sqrt{S}}{2\beta_{\mathrm{l}} p(\beta_{\mathrm{h}} d - \beta_{\mathrm{l}} d)} + \frac{\beta_{\mathrm{h}} \lambda p - c d \delta e^{s\tau}}{p(\beta_{\mathrm{h}} d - \beta_{\mathrm{l}} d)}, \qquad I^* &= -e^{-s\tau} \frac{A - \sqrt{S}}{2\beta_{\mathrm{h}} \beta_{\mathrm{l}} \delta_{\mathrm{p}}}, \\ T_{\mathrm{h}}^* &= \frac{A - \sqrt{S}}{2\beta_{\mathrm{h}} p(\beta_{\mathrm{h}} d - \beta_{\mathrm{l}} d)} + \frac{\beta_{\mathrm{l}} \lambda p - c d \delta e^{s\tau}}{p(\beta_{\mathrm{h}} d - \beta_{\mathrm{l}} d)}, \qquad V^* &= -e^{-s\tau} \frac{A - \sqrt{S}}{2\beta_{\mathrm{h}} \beta_{\mathrm{l}} c \delta}, \end{split}$$

and

$$\begin{split} T_{\mathrm{l}}^{***} &= \frac{A + \sqrt{S}}{2\beta_{\mathrm{l}}p(\beta_{\mathrm{h}}d - \beta_{\mathrm{l}}d)} + \frac{\beta_{\mathrm{h}}\lambda p - cd\delta e^{s\tau}}{p(\beta_{\mathrm{h}}d - \beta_{\mathrm{l}}d)}, \qquad I^{***} &= -e^{-s\tau}\frac{A + \sqrt{S}}{2\beta_{\mathrm{h}}\beta_{\mathrm{l}}\delta_{\mathrm{p}}}, \\ T_{\mathrm{h}}^{***} &= \frac{A + \sqrt{S}}{2\beta_{\mathrm{h}}p(\beta_{\mathrm{h}}d - \beta_{\mathrm{l}}d)} + \frac{\beta_{\mathrm{l}}\lambda p - cd\delta e^{s\tau}}{p(\beta_{\mathrm{h}}d - \beta_{\mathrm{l}}d)}, \qquad V^{***} &= -e^{-s\tau}\frac{A + \sqrt{S}}{2\beta_{\mathrm{h}}\beta_{\mathrm{l}}c\delta}, \end{split}$$

where

$$\begin{split} A &= \quad \beta_{\rm h} c d \delta e^{s\tau} - \beta_{\rm h} \beta_{\rm l} \lambda p \, + \, \beta_{\rm l} c d \delta e^{s\tau} \, + \, \beta_{\rm l} c \delta q e^{s\tau} \, + \, \beta_{\rm h} c \delta r e^{s\tau}, \\ S &= \quad \beta_{\rm h}^2 \beta_{\rm l}^2 \lambda^2 \, p^2 - 2 e^{s\tau} \, \beta_{\rm h}^2 \beta_{\rm l} c d \delta \lambda \, p \, + \, 2 e^{s\tau} \, \beta_{\rm h}^2 \beta_{\rm l} c \delta \lambda \, p r \, + \, e^{2s\tau} \, \beta_{\rm h}^2 c^2 d^2 \delta^2 \\ &\quad + \, 2 e^{2s\tau} \, \beta_{\rm h}^2 c^2 d \delta^2 r \, + e^{2s\tau} \, \beta_{\rm h}^2 c^2 \delta^2 r^2 \, + \, 2 e^{s\tau} \, \beta_{\rm h} \beta_{\rm l}^2 c d \delta \lambda \, p \, + \, 2 e^{s\tau} \, \beta_{\rm h} \beta_{\rm l}^2 c \delta \lambda \, p q \\ &\quad - \, 2 e^{2s\tau} \, \beta_{\rm h} \beta_{\rm l} c^2 d^2 \delta^2 - 2 e^{2s\tau} \, \beta_{\rm h} \beta_{\rm l} c^2 d \delta^2 q \, - \, 2 e^{2s\tau} \, \beta_{\rm h} \beta_{\rm l} c^2 d \delta^2 r \, + \, 2 e^{2s\tau} \, \beta_{\rm h} \beta_{\rm l} c^2 \delta^2 q r \\ &\quad + \, e^{2s\tau} \, \beta_{\rm l}^2 c^2 d^2 \delta^2 + \, 2 e^{2s\tau} \, \beta_{\rm l}^2 c^2 d \delta^2 q \, + \, e^{2s\tau} \, \beta_{\rm l}^2 c^2 \delta^2 q^2. \end{split}$$

4.5 R₀ in Threshold Dynamics: Impact of Intracellular Delay and Morphine

An equilibrium is biologically existent if all of its populations are positive. Figure 3 (left) displays the viral load steady states V^* and V^{**} with respect to R_0 . We clearly see that V^{**} is negative on the whole range of R_0 , and therefore, the equilibrium E^{**} is never biologically existent. V^* is positive for $R_0 > 1$ and the same is true for I^* (data not shown), and since T_1^* and T_h^* are strictly positive for all R_0 , the infected equilibrium E^* is existent for $R_0 > 1$. We also summarize the numerically obtained stability through the bifurcation diagram in Fig. 3 (right). As revealed by our numerical experiment, the stability of the equilibria and hence the dynamics of the model are completely determined by the basic reproduction number R_0 .

Using our parameter estimates, we obtain $R_0 = 2.35$. As $R_0 > 1$, the infection spreads, consistent with the data. We now study how R_0 is affected by the intracellular delay τ . As we are particularly interested in the effect of the intracellular delay in the presence of morphine, we analyze the relation between the basic reproduction number R_0 and the delay τ as well as the relation between R_0 and the morphine-related parameters r and q in greater detail. Figure 4 shows the effects of τ , r, and q on R_0 while



81 Page 14 of 23 N. K. Vaidya, M. Peter

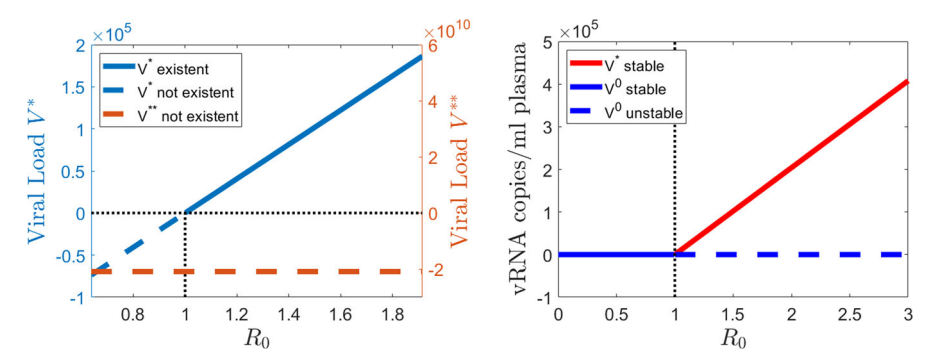


Fig. 3 [Left] Existence of the infected equilibrium E^* . Existence of the infected equilibrium E^* . The viral load steady states of the equilibria E^* and E^{**} are shown with respect to the basic reproduction number, R_0 . If a population is negative, which is shown by a dashed line, it is not biologically existent. [Right] Numerically obtained transcritical bifurcation diagram of steady-state viral load. The steady-state viral load is given by the infection-free equilibrium, E^0 , and the infected equilibrium, E^* . Numerically tested stability of each equilibrium is also indicated with a solid line representing a stable equilibrium and a dashed line representing an unstable equilibrium

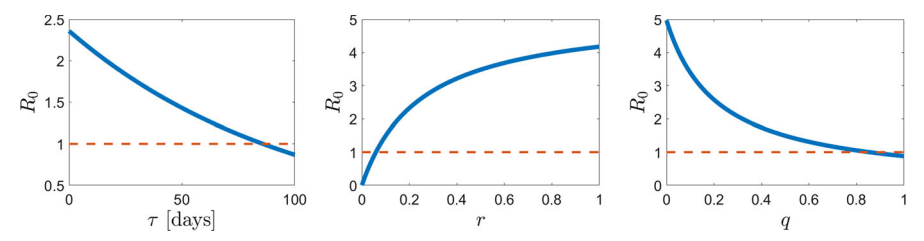


Fig. 4 Dependence of R_0 on τ , r and q. The effect of changing one particular parameter τ , r or q, while keeping all others fixed, on the basic reproduction number R_0 is shown. The dashed line indicates $R_0 = 1$

keeping all other parameters fixed. The expression of R_0 shows that the basic reproduction number is a decreasing function of the delay τ . Therefore, ignoring the delay might overestimate the basic reproduction number. Increasing the delay τ eventually leads to $R_0 < 1$, at which the infection is avoided. For our estimated parameters, this happens at a delay of approximately 86 days (Fig. 4). We note that the delay of 86 days is unrealistic to achieve in general. Nevertheless, the required delay can come down to realistic ranges and might become important in determining whether the infection occurs when we consider treatment, particularly pre-/post-exposure prophylaxis.

Furthermore, we observe that R_0 is significantly affected by changes in r and q. We notice that the presence of morphine, which results in higher r and lower q values, increases R_0 causing further obstacles to control the disease with ART (Fig. 4). We also computed the threshold delay τ^* corresponding to $R_0=1$ for different values of the morphine-related parameters, r and q. We observe that for low values of r and high values of q, i.e., for small amount of morphine presence, small (realistic) values of τ can play a role in determining whether infection occurs $(R_0>1)$ or dies out $(R_0<1)$ (Fig. 5).



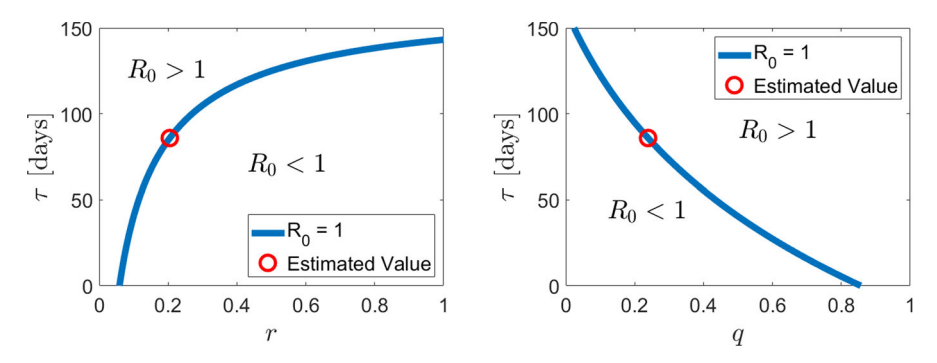


Fig. 5 Dependence of threshold τ^* corresponding to $R_0=1$ on r and q. For parameter combinations of τ and r or q above the curves, $R_0<1$ and the HIV infection dies out, while for parameter combinations below the curves, $R_0>1$ and the infection spreads. The estimated value, drawn as circles, signifies the threshold delay τ^* corresponding to $R_0=1$ based on our current parameter estimates

5 Simulation Results

In this section, we conduct simulations of the developed model to study the effects of morphine concentration and the intracellular delay on the viral load, the CD4 count, and the proportion of target cells with high susceptibility. The effect of morphine can be studied by altering the transition rates r and q between the two subpopulations of target cells in our model. A higher morphine concentration leads to an increase in r and to a decrease in q. The dependency of r and q on the morphine concentration is described by an Emax model of the form (Ting 2006)

$$r(M) = r_c + (r_m - r_c)\eta_r(M),$$

 $q(M) = q_c + (q_m - q_c)\eta_q(M),$

where

$$\eta_r(M) = \frac{M^n}{M_h^n + M^n},$$

$$\eta_a(M) = 1 - \eta_r(M).$$

Here, M represents the concentration of morphine in the blood plasma. Olkkola et al. (1988) measured the kinetics and dynamics of morphine in children and observed peak plasma concentrations of morphine between 135 and 330 microgram per liter. Therefore, we will vary the concentration of morphine, M, between 0 (i.e., no morphine) and 300 μ g/L. r_c and q_c reflect the transition rates in the absence of morphine, which are taken as the values listed in Table 1. $r_m = 0.5$ and $q_m = 4.42 \times 10^{-7}$ are the values of r and q under a high amount of morphine conditioning, as estimated in Vaidya et al. (2016). M_h represents the morphine concentration at which q(M) and r(M) reach the average (midpoint) of their maximum and minimum values. Since there is no information about this value, we assume $M_h = 100 \mu g/L$ for our base



81 Page 16 of 23 N. K. Vaidya, M. Peter

case computation. The Hill coefficient is taken as n = 8, estimated based on in vitro co-receptor expression data.

5.1 Viral Load

Our model predicts that a higher delay, as well as higher morphine concentration, leads to more oscillation in the curve before it reaches a set point, and it takes longer to reach the steady state (Fig. 6). All solutions converge toward the steady state, consistent with the above results (Sect. 4) of the infected equilibrium being asymptotically stable for this parameter set, which gives $R_0 > 1$. The peak of the viral load curve is shifted to the right with increasing τ , i.e., the peak time of the viral load is delayed due to intracellular delay (Fig. 6c). For example, assuming no intracellular delay, the viral load peak occurs approximately 7 days after the infection. In contrast, an intracellular delay of 2 days causes the viral load peak to occur at 32 days post-infection. The viral peak occurs earlier for an increased morphine concentration. However, the impact of morphine on the viral peak time is less intense than the impact of the intracellular delay (Fig. 6c). For example, in the absence of morphine, the viral load peak occurs at 11 days post-infection, whereas it occurs at 7 days with a morphine concentration of 300 μ g/L.

We further observe that the peak value slightly decreases with increasing intracellular delay and increases with the concentration of morphine (Fig. 6d). We notice that the viral load peak value changes are not significant, since the maximum of change is below a half log-scale in each case. In the experimental data (Kumar et al. 2004), there was no significant difference in the viral load peak values regarding the morphine concentration; hence, our model is consistent with this observation in the experimental data.

Regarding the steady-state viral load, there are negligible effects of τ and only small effects of a change in the morphine concentration (Fig. 6e). As presented in the surface plot and the contour plot (Fig. 6e), morphine has a higher effect on the steady-state viral load than the intracellular delay. The steady-state viral load slightly increases with increasing morphine concentration, consistent with experimental data (Kumar et al. 2004). In the absence of morphine, the steady-state level of viral load is 5.4 \log_{10} , while with a morphine concentration of 300 μ g/L, it reaches 5.6 \log_{10} .

5.2 CD4 Count

The CD4 count, which is given by $\frac{T_1+T_h+I}{1000}$ cells per microliter, is often used to measure the HIV patient's immune status. We observe a higher loss for a higher concentration of morphine (to 30 cells per μ L at a morphine concentration of 300 μ g/L vs. to 140 cells per μ L in the absence of morphine, Fig. 7). In addition, with an intracellular delay, the sharp drop in the beginning is also delayed in the model solution, with a slower steady decrease during the lag time. As we found, in the absence of the intracellular delay, the model predicts that the CD4 count drops to 150 cells per μ L, whereas it drops to 115 cells per μ L for an intracellular delay of 2 days.



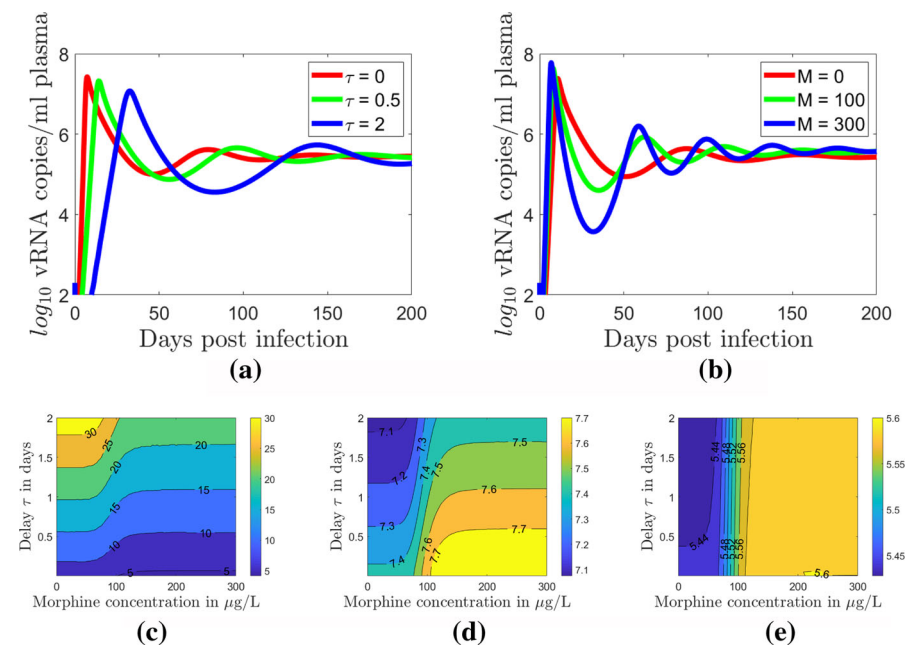


Fig. 6 Viral dynamics predicted by the model for (a) different intracellular delays and (b) different morphine concentrations. (c) Viral load peak for different intracellular delay and morphine concentration. (d) Time to viral load peak for different intracellular delay and morphine concentration. (e) Viral load steady state for different intracellular delay and morphine concentration. The parameters used are the same as in Table 1

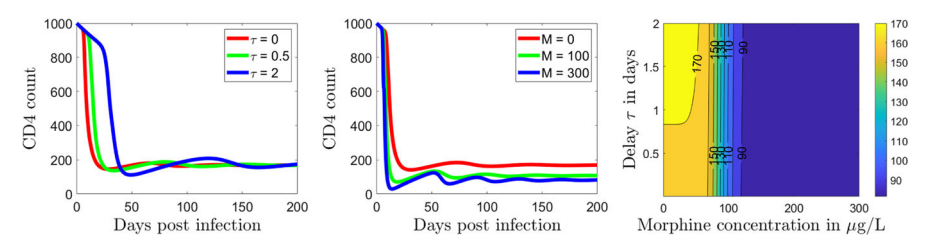


Fig. 7 Model prediction of [Left] the CD4 count dynamics for different intracellular delays, [Middle] CD4 count dynamics for different morphine concentrations, and [Right] the steady-state of CD4 count for the different intracellular delays and morphine concentrations. All the parameters used are the same as in Table 1

The steady-state CD4 count is not affected significantly by the delay (Fig. 7), while the effect of the morphine concentration on the steady-state CD4 count is quite significant. For a high morphine concentration, the model predicts a significantly lower steady-state CD4 count (80 cells per μ L for $M=300 \mu g/L$) than in the absence of morphine (170 cells per μ L), consistent with experimental data (Kumar et al. 2004). Hence, a higher morphine concentration leads to a significantly higher total loss in the CD4 count (92% loss for $M=300 \mu g/L$ vs 83% loss for M=0).



81 Page 18 of 23 N. K. Vaidya, M. Peter

5.3 Proportion of Higher Susceptible Target Cells

We now study how the percentage of higher susceptible target cells, i.e., $(\frac{T_h}{T_l + T_h} \times 100\%)$, are affected by the intracellular delay and morphine concentration. We obtained an early drop in the percentage of higher susceptible target cells (Fig. 8a, b). After this early loss, the T_h -percentage quickly recovers and converges toward its steady state for all parameter sets. The initial drop in the percentage of T_h cells is delayed due to an intracellular delay.

In the early phase of infection, the $T_{\rm h}$ -proportion is significantly affected by the intracellular delay, particularly for a high morphine concentration, as shown by the model predicted $T_{\rm h}$ -percentage at weeks 1, 2, 3, and 4 (Fig. 8c–f). For example, at one-week post-infection, we observe that the $T_{\rm h}$ -percentage increases from about 20% to 40% with increasing delay for small morphine concentrations. In contrast, we observe an increase from 10% to 90% with increasing delay for high morphine concentrations. In general, the intracellular delay has pronounced effects on the $T_{\rm h}$ -percentage in the early phase of HIV infection.

We note that the percentage of higher susceptible target cells, in the long run, is not affected much by the delay (Fig. 8a). However, the morphine concentration significantly affects the steady state T_h -percentage (Fig. 8b). For example, in the absence of morphine (M=0), the steady-state level of T_h -percentage is 43%, whereas, for a morphine concentration of 300 μ g/L, the T_h -percentage reaches 91%.

6 Discussion and Conclusion

Drugs of abuse are known to exacerbate HIV infections, but the exact effects on HIV viral dynamics are not well understood yet, particularly in the context of intracellular delay. In this study, we developed, for the first time, an HIV viral dynamics model that includes the effects of intracellular delay under the conditioning of morphine (a drug of abuse). The intracellular delay, defined as the time in the viral life cycle between the stage of virus entry into the target cell and the stage at which the infected cell produces new viruses, in the presence of morphine is the novel feature of our model. As predicted by the analysis of our model, the intracellular delay significantly affects different aspects of viral dynamics, particularly during early infection. Thus, our study underscores the need for intracellular delay in modeling to accurately predict the effects of morphine on HIV dynamics.

By fitting our model to experimental data from SIV infected macaques, we estimated $\tau=0.231$ days, equivalent to an intracellular delay of approximately 6 hours. The delay estimated by our model is consistent with previous studies (Rong et al. 2007; Kirschner and Webb 1996), in which a value of 0.25 days was used as the maximum age of a cell at which reverse transcription occurs. This value was also used by Alshorman et al. (2017) as an intracellular delay. Furthermore, Mittler et al. (1998) and Dixit et al. (2004) estimated the range of the intracellular delay to be between 0.2 and 1.8 days and between 0.6 and 1.2 days, respectively. Notably, the estimates for the transition rates between subpopulations of target cells are in a similar time scale as the intracellular delay ($r=0.205~{\rm day}^{-1}$ and $q=0.239~{\rm day}^{-1}$). This indicates that many target cells



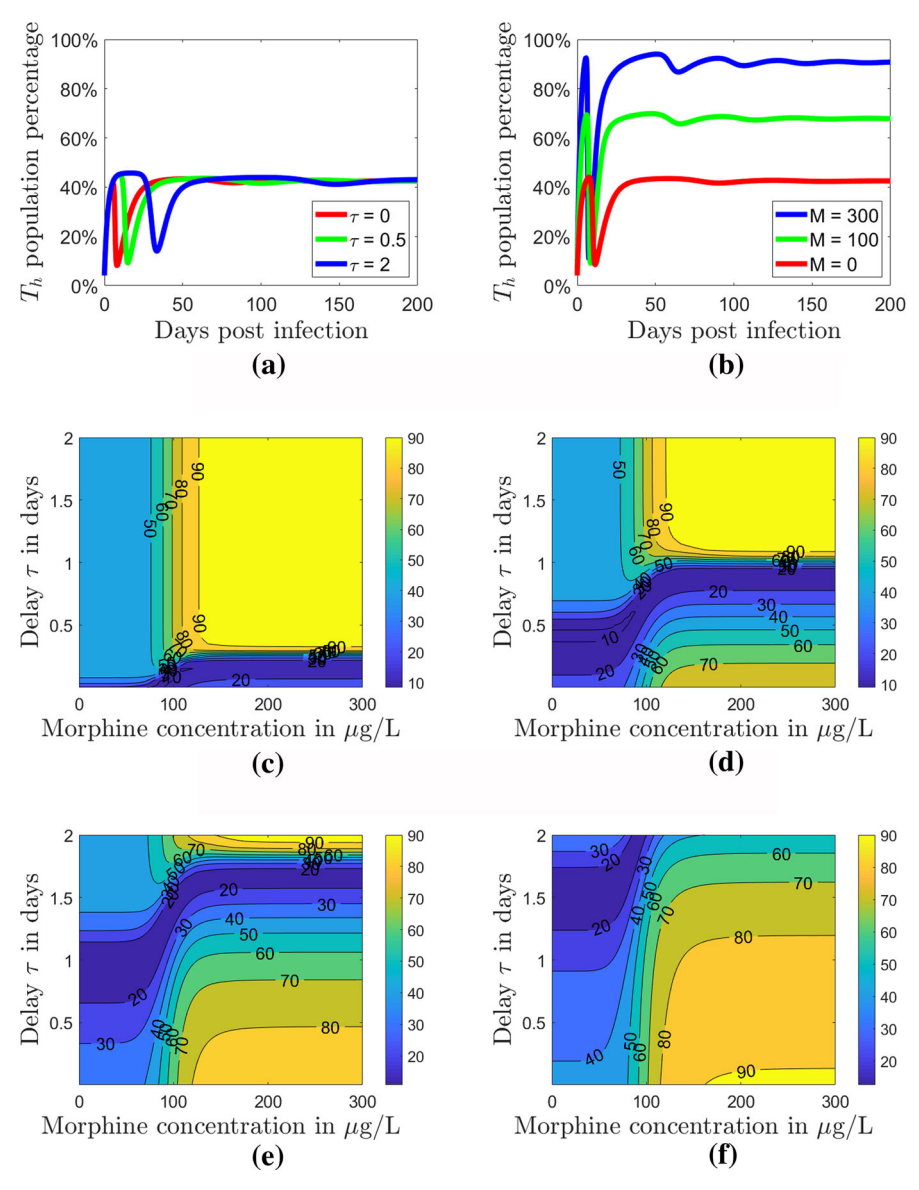


Fig. 8 T_h -percentage dynamics for different intracellular delay and morphine concentration. T_h -percentage dynamics predicted by the model for (a) three selected values of delay (τ) and (b) three selected values of morphine concentration (M). Contour plot of T_h -percentage for various intracellular delay and morphine concentration at (c) week 1, (d) week 2, (e) week 3, and (f) week 4 after the initial infection. The parameters used are the same as in Table 1



81 Page 20 of 23 N. K. Vaidya, M. Peter

might switch between the subpopulations during this intracellular delay, resulting in different amounts of de novo infections, as seen in their dynamics (Fig. 8).

Using our model, we derived the basic reproduction number, R_0 , and showed that the stability of the equilibria and hence the dynamics of the model are completely determined by R_0 . Specifically, our investigations on the model reveal that if $R_0 < 1$, the infection-free equilibrium is asymptotically stable (i.e., the infection is avoided), and if $R_0 > 1$, the infection spreads. We found that an increase in intracellular delay decreases R_0 .

For increasing intracellular delay, there is slower growth in the viral load and a significantly longer time (25 days) to the viral load peak. A high concentration of morphine makes the viral peak reach earlier (19 days). In line with the increased longer time for the viral peak to occur with increasing τ , the immediate loss in the CD4 count and the early drop in the percentage of higher susceptible target cells also take a longer time for increasing intracellular delay. This effect is pronounced on the proportion of higher susceptible target cells. The peak value of the viral load, on the other hand, is not significantly affected by the intracellular delay or the morphine concentration.

In general, a higher intracellular delay or a higher concentration of morphine leads to more oscillation in the solution curves. Nevertheless, the nonzero steady states were eventually reached for all parameter sets, consistent with the results showing the asymptotical stability of E^* . The level of steady state was not significantly affected by changes in the intracellular delay. However, we could observe that a higher morphine concentration leads to a noticeable higher viral set point and a significantly higher total loss in the CD4 count (83% loss of the initial CD4 count in the absence of morphine vs. 92% loss in the presence of a high morphine concentration). These results are consistent with results in earlier studies (Vaidya et al. 2016; Mutua 2018). Furthermore, the T_h -percentage was significantly higher at the steady state with increasing morphine concentration, whereas the intracellular delay has almost no effect on the steady state T_h -percentage.

We acknowledge several limitations of our study. Because of the limited data set, we generated artificial data based on previous models and used them to estimate model parameters. A larger data set would allow us to gain more confidence in the estimated parameter values. As there are no reliable estimates for the death rate of target cells during the intracellular phase, s, we set it to be equal to the death rate of susceptible target cells, i.e., s = d, assuming that the cell remains healthy even after the viral entry until it starts producing new virions. Presumably, the actual value of s might be higher than the death rate of healthy cells due to ongoing viral replication inside these cells. If the death rate is higher during the intracellular delay, the effects of the delay would be even higher than we obtained in this study. Because of highly complex expressions obtained in the model analysis, mainly due to the presence of two types of uninfected cells, we were able to test the stability of infected equilibrium using only numerical techniques with wide parameter spaces.

Since our objective in this study is to provide a first basic model that includes the effects of intracellular delay under morphine conditioning, we made some simplifications in the model. We only considered the effect of morphine on altering co-receptor expression and ignored immune responses, as this is reasonable for early viral dynam-



ics in the first few months post-infection, during which immune responses are largely absent. However, for the long-term analysis of viral dynamics, antibodies should be included in the model as done by Mutua et al. (2019). We also did not include latently infected cells in the model. Moreover, further study could be to include effects of treatment in the model. Note that the effects of treatment can also be modeled using another type of delay, known as the pharmacological delay, which describes the time between ingestion of the drug and its appearance within the cells.

In summary, by analyzing our new HIV dynamics delay model, which includes intracellular delay in the presence of morphine, we found that the intracellular delay can be of significant importance in the initiation of the virus and during the acute phase of infection. Our study highlights the intracellular delay in viral dynamics modeling for the accurate prediction of the effects of morphine on HIV dynamics.

Acknowledgements This work was funded by NSF Grants DMS-1616299 (NKV), DMS-1836647 (NKV), DMS-1951793 (NKV), and DEB-2030479 (NKV) from National Science Foundation, and UGP award (NKV) and the start-up fund (NKV) from San Diego State University. The authors would like to thank Dr. Peter Blomgren for his valuable discussion. MP would like to thank Dr. Hans-Joachim Zwiesler for his support during the Master's double degree program, during which some of the work was carried out. Finally, the authors would like to thank two anonymous reviewers whose suggestions helped improve the paper.

References

Alshorman A, Wang X, Joseph Meyer M, Rong L (2017) Analysis of HIV models with two time delays. J Biol Dyn 11(sup1):40-64

Avert (2018) Global HIV and AIDS statistics. Avert website. https://www.avert.org/global-hiv-and-aids-statistics. Accessed April 2019

Beretta E, Kuang Y (2002) Geometric stability switch criteria in delay differential systems with delay dependent parameters. SIAM J Math Anal 33:1144

Bonhoeffer S, May RM, Shaw GM, Nowa MA (1997) Virus dynamics and drug therapy. Proc Natl Acad Sci 94(13):6971–6976

Busenberg S, Cooke KL (1993) Vertically transmitted diseases, models and dynamics (Biomathematics. 23). Springer, New York

Cai L, Li X, Ghosh M, Guo B (2009) Stability analysis of an HIV/AIDS epidemic model with treatment. J Comput Appl Math 229(1):313–323

Centers for Disease Control and Prevention (2019) HIV in the United States and dependent areas. CDC website. https://www.cdc.gov/hiv/statistics/overview/ataglance.html. Accessed April 2019

Chen HY, Di Mascio M, Perelson AS, Ho DD, Zhang L (2007) Determination of virus burst size in vivo using a single-cycle SIV in rhesus macaques. Proc Natl Acad Sci 104(48):19079–19084

Diekmann O, Heesterbeek J, Metz J (1990) On the definition and the computation of the basic reproduction ratio R_0 in models for infectious diseases in heterogeneous populations. J Math Biol 28:365

Dixit NM, Markowitz M, Ho DD, Perelson AS (2004) Estimates of intracellular delay and average drug efficacy from viral load data of HIV-infected individuals under antiretroviral therapy. Antivir Ther 9(2):237–246

Friedman H, Newton C, Klein TW (2003) Microbial infections, immunomodulation, and drugs of abuse. Clin Microbiol Rev 16(2):209–219

Guo CJ, Li Y, Tian S, Wang X, Douglas SD, Ho WZ (2002) Morphine enhances HIV infection of human blood mononuclear phagocytes through modulation of β -chemokines and CCR5 receptor. J Investig Med 50(6):435–442

Heffernan JM, Smith RJ, Wahl LM (2005) Perspectives on the basic reproductive ratio. J R Soc Interface 2(4):281–293



81 Page 22 of 23 N. K. Vaidya, M. Peter

Herz A, Bonhoeffer S, Anderson RM, May RM, Nowak MA (1996) Viral dynamics in vivo: limitations on estimates of intracellular delay and virus decay. Proc Natl Acad Sci 93(14):7247–7251

- Joint United Nations Programme on HIV and AIDS (2018) Global HIV & AIDS statistics—2018 fact sheet. UNAIDS website. http://www.unaids.org/en/resources/fact-sheet. Accessed April 2019
- Kirschner D, Webb GF (1996) A model for treatment strategy in the chemotherapy of AIDS. Bull Math Biol 58(2):367–390
- Kumar R, Torres C, Yamamura Y, Rodriguez I, Martinez M, Staprans S, Donahoe RM, Kraiselburd E, Stephens EB, Kumar A (2004) Modulation by morphine of viral set point in rhesus macaques infected with simian immunodeficiency virus and simian-human immunodeficiency virus. J Virol 78(20):11425–11428
- Levy JA (1993) Pathogenesis of human immunodeficiency virus infection. Microbiol Mol Biol Rev 57(1):183–289
- Li MY, Shu H (2010) Global dynamics of an in-host viral model with intracellular delay. Bull Math Biol 72(6):1492–1505
- Li Y, Merrill JD, Mooney K, Song L, Wang X, Guo CJ, Savani RC, Metzger DS, Douglas SD, Ho WZ (2003) Morphine enhances HIV infection of neonatal macrophages. Pediatr Res 54(2):282
- Ma ZM, Stone M, Piatak M, Schweighardt B, Haigwood NL, Montefiori D, Lifson JD, Busch MP, Miller CJ (2009) High specific infectivity of plasma virus from the pre-ramp-up and ramp-up stages of acute simian immunodeficiency virus infection. J Virol 83(7):3288–3297
- Markowitz M, Louie M, Hurley A, Sun E, Di Mascio M, Perelson AS, Ho DD (2003) A novel antiviral intervention results in more accurate assessment of human immunodeficiency virus type 1 replication dynamics and T-cell decay in vivo. J Virol 77(8):5037–5038
- Mittler JE, Sulzer B, Neumann AU, Perelson AS (1998) Influence of delayed viral production on viral dynamics in HIV-1 infected patients. Math Biosci 152(2):143–163
- Mutua JM (2018) Modeling HIV-1 infection and immune responses under drugs of abuse. Ph.D. thesis, University of Missouri–Kansas City
- Mutua JM, Perelson AS, Kumar A, Vaidya NK (2019) Modeling the effects of morphine-altered virus specific antibody responses on HIV/SIV dynamics. Sci Rep 9(1):5423
- Nakata Y, Omori R (2015) Delay equation formulation for an epidemic model with waning immunity: an application to mycoplasma pneumoniae. IFAC PapersOnLine 48(18):132
- National Institute on Drug Abuse (2015) Drug and alcohol use—a significant risk factor for HIV. NIDA website. https://www.drugabuse.gov/related-topics/trends-statistics/infographics/drug-alcohol-use-significant-risk-factor-hiv. Accessed April 2019
- Nelson PW, Murray JD, Perelson AS (2000) A model of HIV-1 pathogenesis that includes an intracellular delay. Math Biosci 163(2):201–215
- Nowak M, May RM (2000) Virus dynamics: mathematical principles of immunology and virology. Oxford University Press, Oxford
- Olkkola KT, Maunuksela EL, Korpela R, Rosenberg PH (1988) Kinetics and dynamics of postoperative intravenous morphine in children. Clin Pharmacol Ther 44(2):128–136
- Perelson AS, Ribeiro RM (2013) Modeling the within-host dynamics of HIV infection. BMC Biol 11(1):96
 Ramratnam B, Bonhoeffer S, Binley J, Hurley A, Zhang L, Mittler JE, Markowitz M, Moore JP, Perelson AS, Ho DD (1999) Rapid production and clearance of HIV-1 and hepatitis C virus assessed by large volume plasma apheresis. Lancet 354(9192):1782–1785
- Rong L, Feng Z, Perelson AS (2007) Mathematical analysis of age-structured HIV-1 dynamics with combination antiretroviral therapy. SIAM J Appl Math 67(3):731–756
- Stafford MA, Corey L, Cao Y, Daar ES, Ho DD, Perelson AS (2000) Modeling plasma virus concentration during primary HIV infection. J Theor Biol 203(3):285–301
- Suzuki S, Chuang AJ, Chuang LF, Doi RH, Chuang RY (2002) Morphine promotes simian acquired immunodeficiency syndrome virus replication in monkey peripheral mononuclear cells: induction of CC chemokine receptor 5 expression for virus entry. J Infect Dis 185(12):1826–1829
- The MathWorks Inc. (2019a) dde23. Matlab documentation. https://www.mathworks.com/help/matlab/ref/dde23.html. Accessed April 2019
- The MathWorks Inc. (2019b) fmincon. Matlab documentation. https://www.mathworks.com/help/optim/ug/fmincon.html. Accessed April 2019
- Ting N (2006) Dose finding in drug development. Springer, Berlin



- U.S. Department of Health and Human Services (2017) About HIV & AIDS: what are HIV and AIDS? HIV.gov. https://www.hiv.gov/hiv-basics/overview/about-hiv-and-aids/what-are-hiv-and-aids. Accessed April 2019
- U.S. Department of Health and Human Services (2018a) HIV/AIDS: the basics. AIDSinfo. https://aidsinfo.nih.gov/understanding-hiv-aids/fact-sheets/19/45/hiv-aids--the-basics. Accessed April 2019
- U.S. Department of Health and Human Services (2018b) The stages of HIV infection. AIDSinfo. https://aidsinfo.nih.gov/understanding-hiv-aids/fact-sheets/19/46/the-stages-of-hiv-infection. Accessed April 2019
- U.S. Department of Health and Human Services (2019) HIV basics—U.S. statistics . HIV.gov. https://www.hiv.gov/hiv-basics/overview/data-and-trends/statistics. Accessed April 2019
- Van den Driessche P, Watmough J (2002) Reproduction numbers and sub-threshold endemic equilibria for compartmental models of disease transmission. Math Biosci 180(1–2):29–48
- Vaidya NK, Ribeiro RM, Liu P, Haynes BF, Tomaras GD, Perelson AS (2018) Correlation between Antigp41 antibodies and virus infectivity decay during primary HIV-1 infection. Frontiers Microbiol 9:1326
- Vaidya NK, Ribeiro RM, Miller CJ, Perelson AS (2010) Viral dynamics during primary simian immunodeficiency virus infection: effect of time-dependent virus infectivity. J Virol 84(9):4302–4310
- Vaidya NK, Ribeiro RM, Perelson AS, Kumar A (2016) Modeling the effects of morphine on simian immunodeficiency virus dynamics. PLoS Comput Biol 12(9):e1005127
- Wang Y, Wang X, Ye L, Li J, Song L, Fulambarkar N, Ho W (2012) Morphine suppresses IFN signaling pathway and enhances AIDS virus infection. PLoS ONE 7(2):e31167
- Zhang L, Dailey PJ, Gettie A, Blanchard J, Ho DD (2002) The liver is a major organ for clearing simian immunodeficiency virus in rhesus monkeys. J Virol 76(10):5271–5273
- Zhu H, Zou X (2009) Dynamics of a HIV-1 infection model with cell-mediated immune response and intracellular delay. Discrete Contin Dyn Syst Ser B 12(2):511–524

Publisher's Note Springer Nature remains neutral with regard to jurisdictional claims in published maps and institutional affiliations.

